CFD Study of in-line Zinc Arc Spray

- Parametric Study of Spray Pattern -

Master's Thesis

Hans Peter Bak

Aalborg University Esbjerg
Energy Technology

In compilation of this report, LaTeX is used as writing program. The same program has been used for constructing tables in the report. All pictures taken of the internet, have the appropriate citing.

Energi
Aalborg Universitet Esbjerg
http://www.esbjerg.aau.dk

AALBORG UNIVERSITET
STUDENTERRAPPORT

Titel:
CFD studie af in-line zink arc spray

Tema:
Parametrisk studie af spray mønstre

Projektperiode:
Forårssemester 2019

Projektgruppe:
PECT4-2-F19

Deltager(e):
Hans Peter Bak

Vejleder(e):
Matthias Mandø

Oplagstal: 2

Sidetal: 34

Afleveringsdato:
31. Maj

Abstract:

Denne raport er lavet som et studie med målet at optimere på en zink arc spray for at give en bedre belægnings kvalitet på en substratprofil. Dette studie var lavet ved brug af en CAD model af en emuleret produktionsprocess. Dette inkludere et sprøjte hus som indeholder sprøjte processen, en substratprofil som zinken bliver sprøjtet på, og en luft strøm som skal emulere et ventilations system.
ANSYS Fluent er anvendt som CFD modelleringsværktøj med en partikelstørrelsesfordeling opbygget som en Rosin-Rammler størrelsesfordeling og en partikel frigivelses radius på 0.3 mm. Parameterne som blev undersøgt var sprøjtevinklen på substratprofilen og sprøjteafstanden til profilen.
Ved at undersøgelse effekten af at ændre sprøjtevinklen, blev den optimale sprøjtevinkel fundet til at være 60 grader, da dette resulterede i den bedste dækning of substratprofilen.
Under undersøgelsen af effekten af at ændre sprøjteafstanden, var det muligt at identificere at den optimale sprøjteafstand på 140 mm resulterede i den mest jævnt fordelte dækning af substratprofilen.

AALBORG UNIVERSITY
STUDENT REPORT

Energy
Aalborg University Esbjerg
http://www.esbjerg.aau.dk

Title:
CFD study of in-line zinc arc spray

Theme:
Parametric study of spray pattern

Project Period:
Spring semester 2019

Project Group:
PECT4-2-F19

Participant(s):
Hans Peter Bak

Supervisor(s):
Matthias Mandø

Copies: 2

Page Numbers: 34

Date of Completion:
31st of May

Abstract:

This report is made as a study to optimize upon a zinc arc spray to give a better coating quality on a substrate profile. The study was made using a CAD model of an emulated production process including a housing for the spraying process, a substrate profile that the zinc is sprayed upon, and an air flow that emulates a ventilation system.
ANSYS Fluent is used as the CFD modeling tool, with a particle size distribution constructed as a Rosin-Rammler size distribution and a particle release radius of 0.3 mm. The parameters that were investigated was the spray angle onto the substrate profile and the spray distance to the profile.
From the investigation of the effect of changing the spray angle, it was found that the optimal angle would be a spray angle of 60 degree as this resulted in the best coverage of the substrate profile.
With the investigation of the effect of changing the spray distance, it was determined that a spray distance of 140 resulted in the most evenly distributed coating coverage of the substrate profile.

Preface

This report was written by group PECT4-2-F19 as the Master's Thesis on 4th semester Process Engineering and Combustion Technology master of science program at Aalborg University Esbjerg 2019.

The report uses Autodesk Fusion 360 as a computer aided design (CAD) tool for the construction of model, and ANSYS Fluent v. 19.2 has been used as the computational fluid dynamics modeling tool.

Aalborg University Esbjerg, May 31, 2019

Hans Peter Bak
hbak14@student.aau.dk

Table of Contents

1 Introduction

Some car manufacturing industries uses an substrate profile coated with zinc which can be used for heat transferring. The coating is required to have a certain quality with a minimum waste of coating material. This coating process can be done through the use of a twin wire electric arc spray gun, which can be seen in figure 1.1.

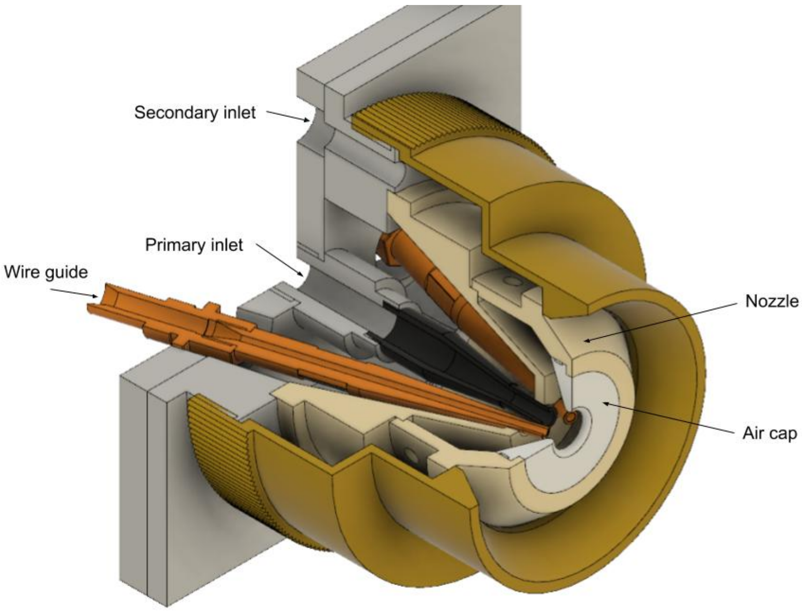

Figure 1.1: CAD model of the twin wire electric arc spray gun

The twin wire electric arc spraying process is a cheap coating method with a high deposition rate that can be used as a thermal spraying process of both ferrous and non-ferrous alloy coating that can be used for various applications [1, 2, 3]. The deposition material is fed through an anode and cathode as two wires and introduced into an electric arc where it is heated. Acting upon the electric arc is a high velocity gas jet, which acts as the driving force to propel the molten material towards the substrate profile. The molten material is atomized into small droplets by the gas jet and is cooled down during its travel and solidifies upon contact with the substrate to form a coating [4, 5, 6]. The concept described here can be seen in figure 1.2. The nozzle and air cap helps guide and form the airflow when it leaves the spray gun. It is a process that is especially suited for spraying large areas as the process is attributed to have a low running cost and high spray rate [7, 5].

The coating process is often used to give protection as a thermal barrier, for wear resistance, corrosion resistance for both high and low temperature corrosion and atmospheric corrosion, giving a high dielectric strength, being a hard dense coating, or just used as a tool for decorative arts [2, 8, 7, 6].

A complication that can occur due to the usage of the twin wire arc spray process is that the particles that are generated tends to be larger in size and have an irregular size distribution, when compared to powder fed thermal spray coating processes, which gives a lower density coating [7]. Though it has a stronger and

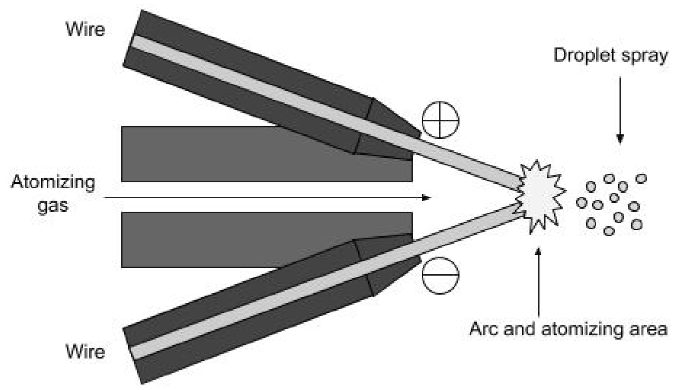

Figure 1.2: Schematic showing the concept of an electric arc spray process

denser coating than combustion spray coatings as described by Wang et al. [5]. Because of this irregularity of the size distribution, an increase of the porosity of the deposit can be found. It has been found to be roughly 6-9% more porous than other thermal spray processes [4].
The twin wire electric arc spray gun has throughout resent years seen an increase in technological development. The reason for this is that the efficiency of this coating technology has received an increased in interest due to required process parameters being able to be covered by the properties of the coating [1].

In different studies it has been shown that changing different parameters can improve the efficiency and the required coating quality for a given product.
Toma et al. [1] describes that using a higher speed of the gas flow produces finer particles carrying a high velocity. This gives the possibility of obtaining a more dense coating with improved properties. A high speed zone is described to occur in the jet when subjected to a convergence nozzle. Through this study it was determined using finite element analysis that having the high speed zone placed to overlap the wielding zone of the electric arc gave an increase in coating quality.

In the study of Chen et al. [3] it is described that a high atomizing gas flow rate and velocity has been shown to increase the droplet velocity and decrease in the mean droplet size, as this can increase the coating quality. This could be observed in a converging/diverging nozzle when compared to cylindrical nozzle. Introducing a secondary gas injection, which acts like a shroud around the main atomizing gas injection. This has shown to increase the particle velocity and significantly decrease the droplet divergence occurring. In regards to any oxidation it can be controlled, to a low degree, through the usage of nitrogen and carbon dioxide. Although this does increase the cost of the spray process.

Gedzevicius et al. [2] investigated the effect that different nozzle geometries has on the particle diameter, through both numerical calculation using the PHOENICS code and experimental testing. It was deemed possible to increase the speed of particles by about 20% and kinetic energy of particles impacts by about 40%.

When looking to the coating material of zinc. It can be found that zinc is often used as a coating material due to it being more electrochemically active than steel. This means that the material that will corrode and the product of this corrosion leaves an insoluble shell that is able to protect the substrate and inhibits any further corrosion to some extent [7]. Using zinc as the coating material is, among others, used in infrastructures such as highways and bridges. It is a coating process primarily used to improve the life cycle cost of a given product [7].

A drawback that is normally associated with arc spraying is its low density coating. This does not make itself present when using zinc-rich powder coatings, as it does not require any special installations. Besides this it is able to be applied in more aggressive media such as water, marine and industrial environments [7].

An area that has not been investigated thoroughly is optimization, when operating under conditions simulating the work environment. In this study a simulation with a arc spray gun placed inside a box spraying onto a surface emulating the substrate profile. In addition to this an air flow is introduced to emulate having ventilation as part of this model. The ventilation is implemented to investigate the effect that this has on the spraying process and thereby the amount of wasted zinc.

2 Problem Statement

This study seeks to optimize the coating process of an existing twin wire electric arc spray gun to minimize the amount of waste material and thereby reduce production costs. This is done through a constructed CAD figure that emulates a possible work environment. Using this figure numerical calculations are made with the use of ANSYS Fluent as a CFD modeling tool.

These areas that are areas of interest that can be investigated:

- The effect of changing the distance the spray gun has to the sprayed upon surface
- The effect of changing the angle the spray gun has to the sprayed upon surface
- If changing the wire angle has an effect on the particle spread.
- The effect the nozzle angle and its distance to the wire has on the particle spread.
- Shape the air cap to change the air flow for a possible optimization of the particle spread

Due to time constraints and limited resources this study will focus on investigating the effect of changing the distance and angle the arc spray gun has to the substrate profile is sprayed upon.

3 Modeled Geometry and Mesh

The simulation model was built in Autodest Fusion 360. This model was made to imitate an existing production process. It consist of having the arc spray gun placed in the corner of a housing container with the substrate profile in the middle of it and a symmetry axis going through the middle of the model. From the end, where the arc spray is, an air inlet is implemented to drive the air towards the outlets on the opposite side this is done to try and emulate a real life ventilation system that could be used in this industry. The setup can be seen in 3.1.

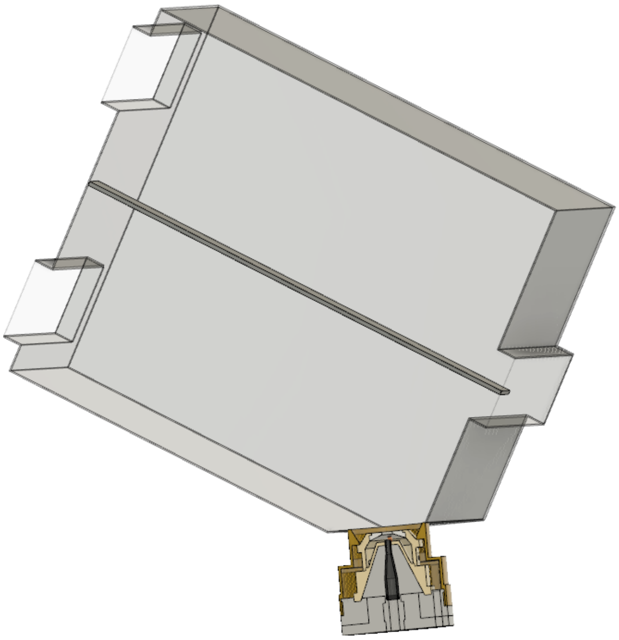

Figure 3.1: CAD model of the arc spray gun within a housing area with a 3 cm profile

The constraints that are to be investigated, highlighted in figure 3.2, are the distance from the arc spray gun has to the substrate profile and the angle the spray gun has the substrate profile.

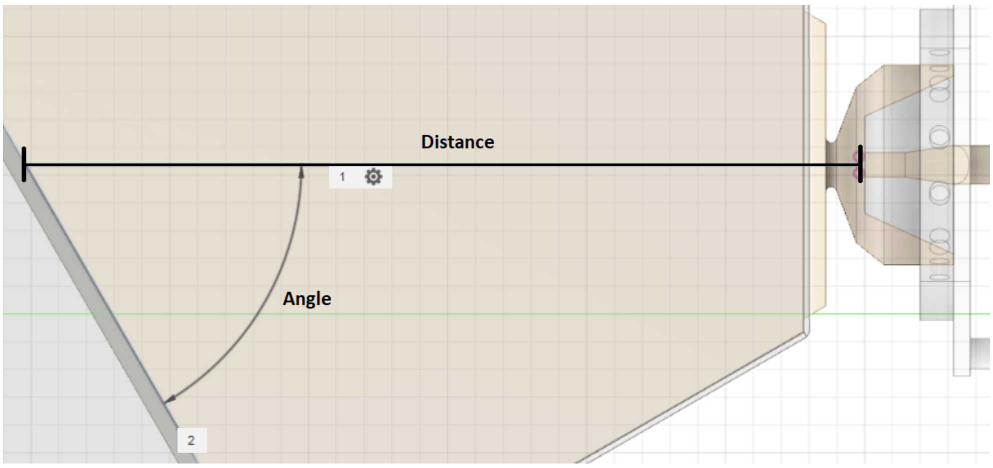

Figure 3.2: A sketch showing the angle an distance that are to be investigated

The meshing type that has been chosen for this model is a tet-mesh and contains 406423 cells. The mesh is shown in figure 3.3. It would be optimal to have constructed a quad-mesh, but this had some complications as the quality of the cells were outside the required values when working in a quad-mesh.

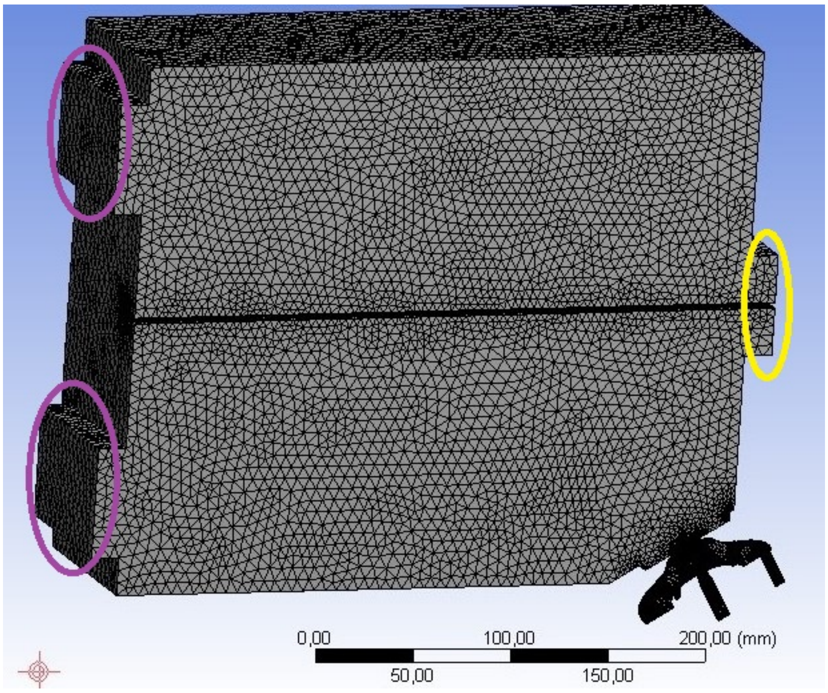

Figure 3.3: The generated tet-mesh of the model. The yellow circle shows the air inlet and the two purple circles show the outlets

For the mesh some simplifications were made inside the arc spray gun since it has a relatively complex geometry, this can be seen in figure 3.4. This was done because of limitations connected to the student version of Fluent, as there are limitations to the amount of cells that can be worked with.

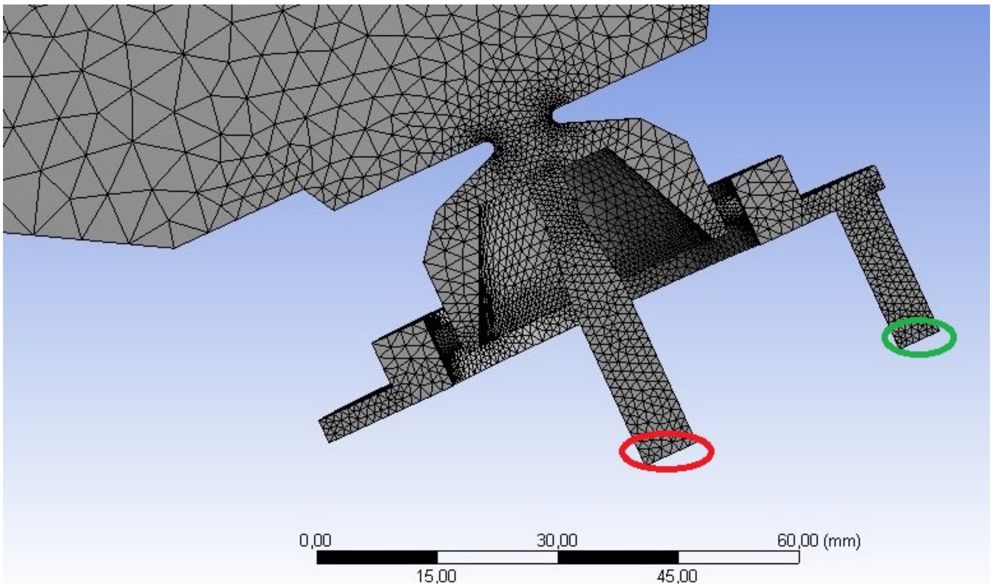

Figure 3.4: A zoom in on the meshed spray gun. The red circle shows the primary inlet and the green circle shows the secondary inlet

In table 3.1 some quality parameters of the final mesh can be seen. This mesh is found in the mesh independency study in chapter 5.1. For the skewness, having a maximum value of 0.60 for a tet-mesh is acceptable as a tet-mesh with a skewness of under 0.9 can seen as being sufficient.
For the aspect ratio “ERCOFACT - Best Practive Guidelines” describes that it should be below 20 - 100, dependent on the flow solver. This model has a maximum aspect ratio of 4.22 which can be considered decent.

Table 3.1: Skewness of the mesh

	Min.	Max.	Average
Skewness	0.00034	0.60	0.24
Aspect Ratio	1.16	4.22	1.86

4 Computational Fluid Dynamic Modeling

To simulate the flow in this study, the software used is ANSYS Fluent version 19.2. The modeling will be centered around the use of Reynolds Average Navier-Stokes (RANS) to compute the flow pattern. RANS is chosen due to the required computational resources, time and that the student version is used. Any possible trade off in accuracy is deemed sufficient, which has been validated through Hooff et al. [9].
The main considerations made for the flow are as following:

- Steady state flow
- Incompressible flow
- The flow is considered one way coupled. Will be expanded on page 12

RANS consists of four equations. The continuity equation 4.1 is related to mass transfer. The 3 Navier-Stokes equations 4.2, 4.3, and 4.4 all relate to momentum.

$$\frac{\partial u}{\partial x} + \frac{\partial v}{\partial y} + \frac{\partial w}{\partial z} = 0 \tag{4.1}$$

$$\rho\Big(u\frac{\partial u}{\partial x} + v\frac{\partial u}{\partial y} + w\frac{\partial u}{\partial z}\Big) = -\frac{\partial P}{\partial x} + \frac{\partial \tau_{xx}}{\partial x} + \frac{\partial \tau_{xy}}{\partial y} + \frac{\partial \tau_{xz}}{\partial z} + \rho g_x \tag{4.2}$$

$$\rho\Big(u\frac{\partial v}{\partial x} + v\frac{\partial v}{\partial y} + w\frac{\partial v}{\partial z}\Big) = -\frac{\partial P}{\partial y} + \frac{\partial \tau_{xy}}{\partial x} + \frac{\partial \tau_{xy}}{\partial y} + \frac{\partial \tau_{yz}}{\partial z} + \rho g_y \tag{4.3}$$

$$\rho\Big(u\frac{\partial w}{\partial x} + v\frac{\partial w}{\partial y} + w\frac{\partial w}{\partial z}\Big) = -\frac{\partial P}{\partial z} + \frac{\partial \tau_{xz}}{\partial x} + \frac{\partial \tau_{yz}}{\partial y} + \frac{\partial \tau_{zz}}{\partial z} + \rho g_z \tag{4.4}$$

In these equations the u, v, and w describes the velocity components in the x, y, and z direction respectively. ρ is the fluid density. The pressure is described as P. g is the gravitational acceleration. τ describes the shearing stresses.

To acquire RANS a Reynolds decomposition of the velocity can be done making an average and fluctuating term $u = \bar{u} + u'$. The RANS equation can be seen in equation 4.5 and is only shown for one dimension.

$$\begin{split}\rho\bar{u}\Big(\frac{\partial \bar{u}\bar{u}}{\partial x} + \frac{\partial \bar{u}\bar{v}}{\partial y} + \frac{\partial \bar{u}\bar{w}}{\partial z}\Big) = -\frac{\partial P}{\partial x} + \frac{\partial}{\partial x}\Big(\mu + \mu_t\big(\frac{\partial u}{\partial x} + \frac{\partial x}{\partial x}\big)\Big) \\ + \frac{\partial}{\partial y}\Big(\mu + \mu_t\big(\frac{\partial u}{\partial y} + \frac{\partial v}{\partial x}\big)\Big) + \frac{\partial}{\partial z}\Big(\mu + \mu_t\big(\frac{\partial u}{\partial z} + \frac{\partial w}{\partial x}\big)\Big) + \rho g_x\end{split} \tag{4.5}$$

Here the μ_t describes the turbulent viscosity and μ is the viscosity.

When dealing with the Reynolds average approach to turbulence modeling. It required that the Reynolds stresses in equation 4.5 can be appropriately modeled. To do this the Fluent Theory Guide recommends the Boussinesq hypothesis that details the ability to relate the Reynolds stresses to the mean velocity gradients as seen in equation 4.6.

$$-\rho\bar{u'}\bar{v'} = \mu_t\left(\frac{\partial u}{\partial y} + \frac{\partial v}{\partial x}\right) \tag{4.6}$$

Because the flow in this model has a Reynolds number at the inlets being from 15000 and 40000 dependent on which inlet the number is calculated. This means that a laminar flow model can not be sufficient for the system.

The model that will be used for these calculations are realizable k-epsilon with standard wall functions. The realizable k-epsilon model differs from the standard k-epsilon model by having an alternative formulation for turbulent viscosity and a modified transport equation for the dissipation rate. This makes it more capable of working with complex structures. The transport equation for k and ε in the realizable k-epsilon are seen in equation 4.7 and 4.8.

$$\frac{\partial \rho k}{\partial t} + \frac{\partial \rho k v}{\partial y} = \frac{\partial}{\partial y}\left[\left(\mu + \frac{\mu_t}{\sigma_k}\right)\frac{\partial k}{\partial y}\right] + G_k + G_b - \rho\varepsilon - Y_M + S_k \tag{4.7}$$

$$\frac{\partial \rho \varepsilon}{\partial t} + \frac{\partial \rho \varepsilon v}{\partial y} = \frac{\partial}{\partial y}\left[\left(\mu + \frac{\mu_t}{\sigma_\varepsilon}\right)\frac{\partial \varepsilon}{\partial y}\right] + \rho C_1 S_\varepsilon - \rho C_2 \frac{\varepsilon^2}{k + \sqrt{v\varepsilon}} + C_{1\varepsilon}\frac{\varepsilon}{k}C_{3\varepsilon}G_b + S_\varepsilon \tag{4.8}$$

with:

$$C_1 = max\left[0.43, \frac{\eta}{\eta + 5}, \eta = S\frac{k}{\varepsilon}, S = \sqrt{2S_{xy}S_{xy}}\right. \tag{4.9}$$

In these equations G_k describes the generation of turbulence kinetic energy as a product of the mean velocity gradients. The G_b describes the generation of turbulence kinetic energy that appears due to buoyancy. σ_k and σ_ε are turbulent Prandtl numbers for k and ϵ respectively. Y_M describes the contribution of the fluctuating dilatation in compressible turbulence to the overall dissipation rate. C_2 and $C_1\varepsilon$ are constants.

For equations related to particle motions the particle force balance can be described as equation 4.10. Some simplifications has been made since the ratio of the continuous phase density and the droplet material density is smaller than 10^{-3}.

$$\frac{d\overrightarrow{u_p}}{dt} = \frac{\overrightarrow{u} - \overrightarrow{u_p}}{\tau_r} + \overrightarrow{g} \tag{4.10}$$

Here the particle velocity is described as $\overrightarrow{u_p}$, ρ_p is the particle density, τ_r describes the particle relaxation time.

4.1 Particle Distribution

To emulate the expected particle distribution that will occur for the zinc particles when leaving the spray housing a Rosin-Rammler distribution is used. The Rosin-Rammler distribution is commonly used to represent droplet size distributions in sprays as described by Crowe et. al [10]. It can be expressed in terms of the cumulative mass distribution as seen in equation 4.11.

$$F_m(d) = 1 - exp\Big[-\Big(\frac{d}{\delta}\Big)^n\Big] \tag{4.11}$$

Here δ and n are two empirical constants describing the characteristic diameter and spread respectively. It can be noted that $F_m(0) = 0$ and $F_m(\infty) = 1$. The empirical constant are determined through plotting the cumulative distribution on log-log coordinates. Introducing the logarithm to equation 4.11 gives equation 4.12.

$$ln[-ln(1 - F_m(D))] = n \cdot ln(D) - n \cdot ln(\delta) \tag{4.12}$$

The line that can be plotted from $-ln[1 - F_m(D)]$ in respect to the diameter on log-log axes is able to provide n as the slope of this line. The δ parameter can be obtained through n and the mass median diameter as shown in equation 4.13.

$$\delta = \frac{D_m M}{0.693^{\frac{1}{n}}} \tag{4.13}$$

Mass frequency distribution can be obtained through taking the derivative of the cumulative distribution as seen in equation 4.14.

$$f_m(D) = \frac{dF_m}{dD} = e^{(-\frac{D}{\delta})^n} \frac{n}{\delta}\Big(\frac{D}{\delta}\Big)^{n-1} \tag{4.14}$$

4.1.1 Particle Implementation

For the particle implementation the discrete phase model is used with the implementation of an interaction with the continuous phase. This implementation is activated after the continues phase and flow field is converged. The physical model that is activated is the Erosion/Accretion model. This is activated because the accretion rate on the wall acting as the substrate profile is of interest for this study.
The particles are released as shown in figure 4.1. The injection is made as a solid cone consisting of ten particle streams. The particles are released with no releasing angle or velocity magnitude. This makes it so that the particles are fully driven by the flow coming from the primary and secondary inlet streams. The diameter of the cone are varied to emulate the spray width of the arc spray gun which will be further elaborated. The amount of diameters that are released are 10 particle diameters from 10 different streams and 10 repetitions that follows a discrete random walk model. This gives $10 \cdot 10 \cdot 10 = 1000$ particle trajectories.

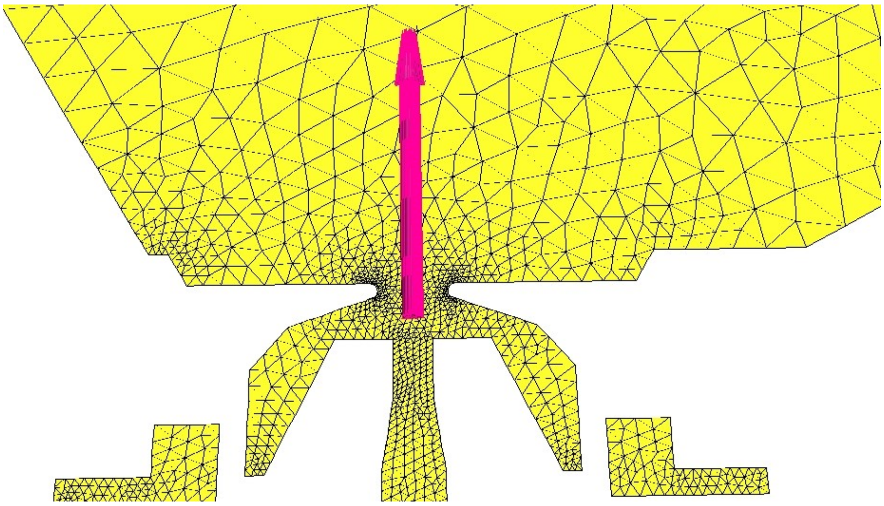

Figure 4.1: Zoom in on the particle spawn point (here shown as a vector) in the CFD model

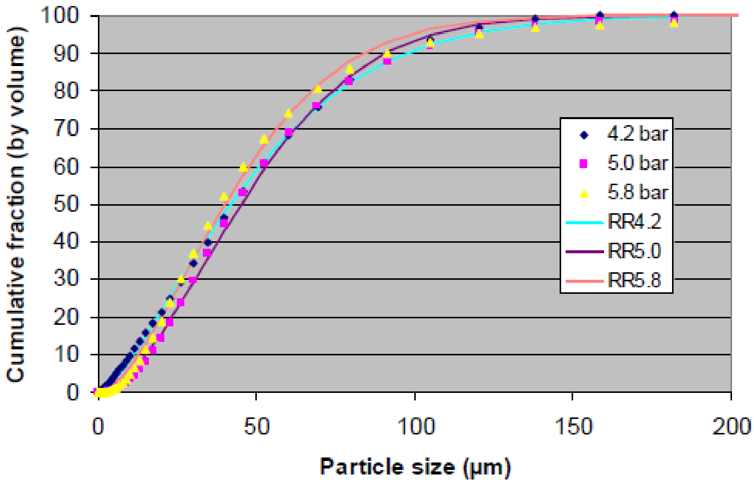

Figure 4.2: Particle size distribution for the zinc particles leaving the arc spray gun and the effect of using different pressure on the particle [11]

In this study a Rosin-Rammler size distribution is used for the zinc particle sizing. This data given from an experiment made by Bolot and Verdy [11]. In this experiment the zinc particles are sprayed into water and a corresponding size distributions were analyzed through a laser granulometer. From the analysis it was observed that the collected particles were distorted, most likely from the particles initial contact with the water. The results from this experiment can be seen in figure 4.2 and shows that increasing the atomizing gas pressure has a small effect on the particle size. Having a higher pressure shows a small tendency to produce smaller particles. In table 4.1 are shown the parameters that makes up the Rosin-Rammler size distribution, which will be used in the CFD study. It shows the minimum diameter of the particles being created, the maximum particle diameter, the mean particle diameter, and the spread parameter of the particle diameters.

Table 4.1: Particle size distribution for the zinc particles

Min. Diameter	Max. Diameter	Mean Diameter	Spread Parameter
0.001	0.175	0.0543	1.42

4.2 Mass loading

To determine if the phase coupling is one way or two way coupled the mass loading is to be calculated. This is calculated from the ratio of mass flux of the dispersed phase, $\dot{m}_d$, to the continuous phase, $\dot{m}_c$, which is seen in figure 4.15.

$$z = \frac{\dot{m}_d}{\dot{m}_c} \tag{4.15}$$

When calculating this using a mass flux for the dispersed phase of 0.02 kg/s and 0.38 kg/s from the air inlet a mass loading of 0.05 can be calculated. From Clayton et. al. [12] it was described that having a particle diameter of 0.0543, as average, and a mass loading of 0.05 would result in a dilute flow region. Having a dilute flow makes it possible to consider the phase coupling to be one way coupled.

4.3 Models and Methods

The Fluent solver has a plethora of available solving methods to calculate the flow of a system. To identify which are best to implement in this system the ANSYS User's Guide was used to compare these methods.

4.3.1 Pressure-/ Density-based solver

The pressure based solver is commonly used for low velocity incompressible flows, whereas the density based solver can be used in compressible flows at high velocities. The pressure based solver includes a pressure correction equation that finds the pressure field through manipulation of the continuity and momentum equation. The density based solver finds the pressure field through the use of continuity, which can give the pressure field through the equation of state. In common for both solvers is that they obtain the velocity field from the momentum equations.

This system aims to work with a flow field where the velocity is expected to be below $Ma = 0.3$. This gives reason to assume that the air is acting as an incompressible flow. Therefore it can be observed that the pressure-based solver would best suit this system.

4.3.2 Coupled/decoupled method

For the governing equations that aims to solve the pressure correction equation can be non-linear or coupled to each other and has to be solved iteratively. This can be calculated separately for each governing equation (decoupled), or they can be calculated simultaneously (coupled). For the coupled method it can be expected to use 1.5 to 2 times more computational memory because the method stores the discrete system while calculating the velocity and pressure fields. Even though this method requires more memory, it can be expected to converge faster than the decoupled algorithms.

SIMPLEC
When working with a laminar flow problem the SIMPLEC algorithm excels and can be used with no other models enabled and the convergence is limited through the pressure-velocity coupling.

PISO
The PISO algorithm are recommended for transient flow calculations. As this system is considered steady state, then PISO will not be an optimal solver.

Coupled
The coupled scheme (in earlier Fluent versions known as Multiphase Coupled) solves for all equations for phase velocity corrections and shared pressure correction simultaneously. This method work well in steady state situations, or for transient problems where a larger time step is required.

Because the couple scheme works with multiple phases, it will be used for this system.

4.3.3 Spatial Discretization

Gradient has the options of being Green-Gauss Based, Green-Gauss Node Based and Least Squares Cell Based. In the Fluent User's Guide there is not described any significant differences, though Least Squares Cell Based gradient is the cheapest from a computational viewpoint.

Pressure has the Second Order setting is used by default. Linear and Standard requires a smooth pressure gradient which makes it ineffective when working with high pressure gradients. Body Forces Weighted works with forces such as buoyancy being applied. Presto! works well for Volume of Fluid calculations which works well with multiphase flow with a fluid-fluid interface.

Momentum and Turbulence with First Order Upwind works well with flows that are aligned with the mesh as numerical diffusion will not appear. It has the tendency of having a good convergence even for meshes with a bad quality, though numerical diffusion and low accuracy can appear, when working with a complex flow.
The Second Order Upwind has qualities like First Order Upwind. The Fluent User's Guide recommends starting with the First Order Upwind scheme and then switching to a higher order scheme.
For the QUICK and 3rd Order MUSCL it will give a better accuracy, when dealing with rotating and swirling flows.

The second order upwind scheme for momentum was firstly used for this system. It showed to have some difficulties, when an interaction with the continuous phase for the released particles was implemented. This could be a consequence of the lower quality of the mesh. Therefore the first order upwind setting was selected for both momentum and turbulence.

4.4 Boundary Conditions

The boundary conditions for the walls in the model has been changed to have the discrete phase model conditions to be trapping. This traps all particles that come into contact with the wall.

For the air flow coming from the arc spray gun shown in 4.3 the velocity for the primary and secondary inlet streams are taken from an internal report. Since the velocities from the report are shown as a contour figure with a given color range, the velocity is set to a velocity within these ranges.

For the primary inlet the velocity magnitude is given to be 65 m/s and has a turbulence given by a turbulence intensity of 5 percent and a hydraulic diameter of 3.47 mm.

For the secondary inlet a velocity magnitude of 120 m/s is given and a turbulence intensity of 5 percent and a hydraulic diameter of 2.7 mm.

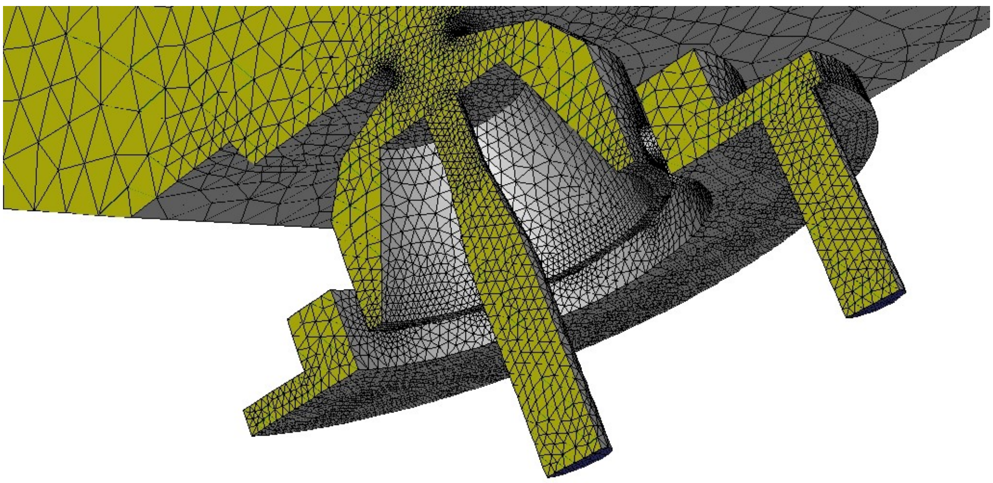

Figure 4.3: Zoom in on the primary (middle of the picture) and secondary (right) inlet jets of the arc spray gun. The figure is seen from the models symmetry plane

Because the model is trying to simulate a ventilation system an air inlet is implemented with a velocity magnitude of 60 m/s to emulate an air flow that would result from the ventilation.

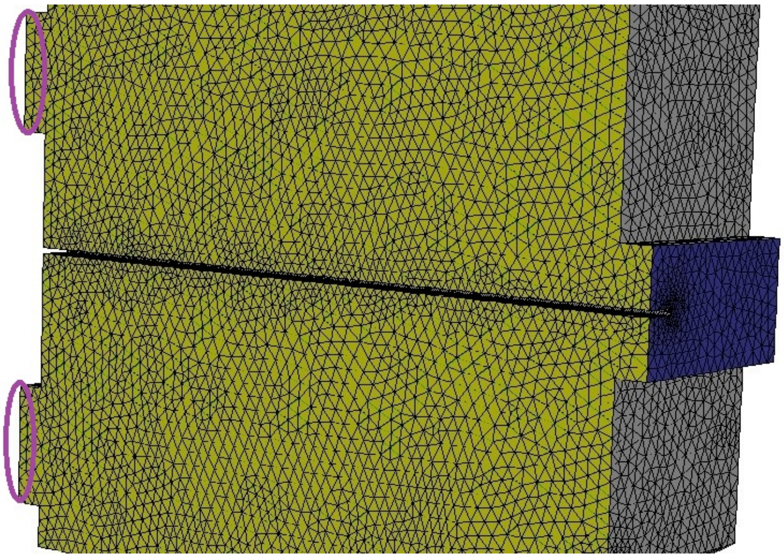

Figure 4.4: A zoom in on the CFD model showing the air inlet on the right (shown in blue) and the outlets on the left (the two purple circles). The figure is seen from the the models symmetry plane

5 Results

5.1 Mesh Independency Study

To identify an estimate of an optimal refinement a mesh independency study is made. The values that are to be investigated are the amount of iterations until the continuous phase and flow field is converged, and the continuity value. A table of these values can be seen in table 5.1 and a residual plot can be seen in figure 5.1.

Table 5.1: Mesh independency study

Number of cells	Iterations until convergence	Continuity value
499375	≈ 1000	$1.94 \cdot 10^{-}7$
406423	≈ 900	$1.61 \cdot 10^{-}7$
357793	≈ 500	$4.10 \cdot 10^{-}6$
313085	≈ 800	$5.50 \cdot 10^{-}7$
209431	≈ 500	$3.09 \cdot 10^{-}6$

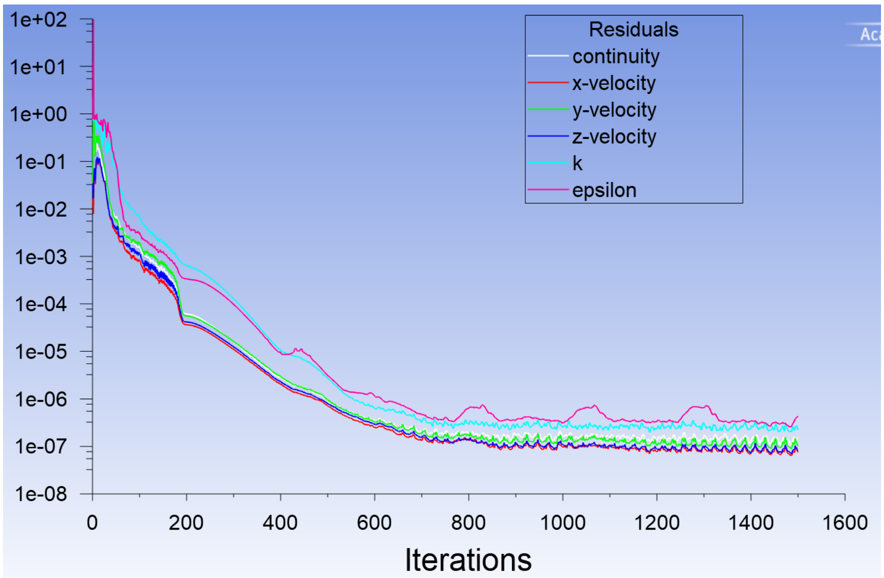

Figure 5.1: Graph showing the residual values for a mesh of 406423 cells

In respect to the approximated iterations until convergence general tendency can be seen. As the amount of cells increase the required amount of iterations also increase, though a drop appears from 313085 cells to 357793 cells.
With the continuity value a general tendency can be likewise be observed, with the continuity value decreasing as the amount of cells are increased. As with the iteration number an increase appears from 313085 cells to 357793 cells. Besides this the change from 406423 to 499375 cells has a small increase which can be observed.

From these values it can be determined that the mesh containing 406423 cells has the possibility to be the most accurate of the constructed meshes. It can be seen that it does not require a too significant amount of iterations to reach convergence and the continuity value is the lowest of the used meshes.

5.2 Particle injection study

To be able to fully emulate the particle spray a study into the particle spray width has been made. From a spray test, as seen in figure 5.2, it can be observed that a spray width close to 3 cm can been achieved with the coating on the edge being less dense. Considering that the substrate profile has a width of 3 cm it will be used for evaluating if the spray width has been achieved in the CFD model. The test was made under operating conditions using cardboard as the substrate and with three spray guns activated.

Figure 5.2: Spray test of zinc sprayed on cardboard from three arc spray guns

The way this spray width is tried to be emulated is through changing the particle release radius of the spawn point from 0.1 mm to 0.5 mm. In figure 5.3 a radius of 0.1 mm has been used. It shows the particle trajectories. From the figure it can be seen how some of the trajectories are captured by the profile showed in a zoom in as seen in figure 5.4 and that smaller particles are moving past the profile. This observation repeats for all simulations. Since the capture of the particles are the area that is of interest only a zoom in on the profile will be shown going forward. In figure 5.5 a histogram of the captured particles are shown in percentages with the x-axis being the width of the substrate profile with zero marking the symmetry plane. It shows that the majority of the particles are captured close to the middle of the profile.

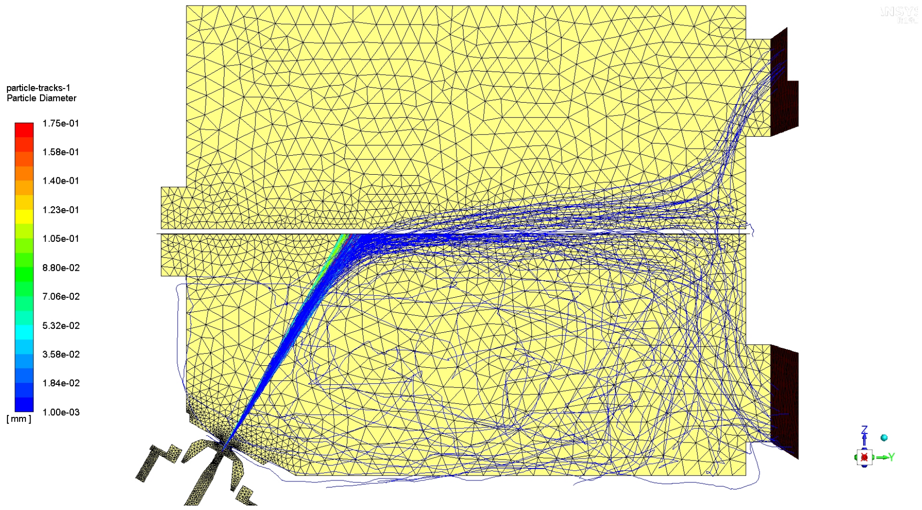

Figure 5.3: Depiction of the particle trajectories in the simulation with a particle release radius. The yellow wall is the symmetry plane.

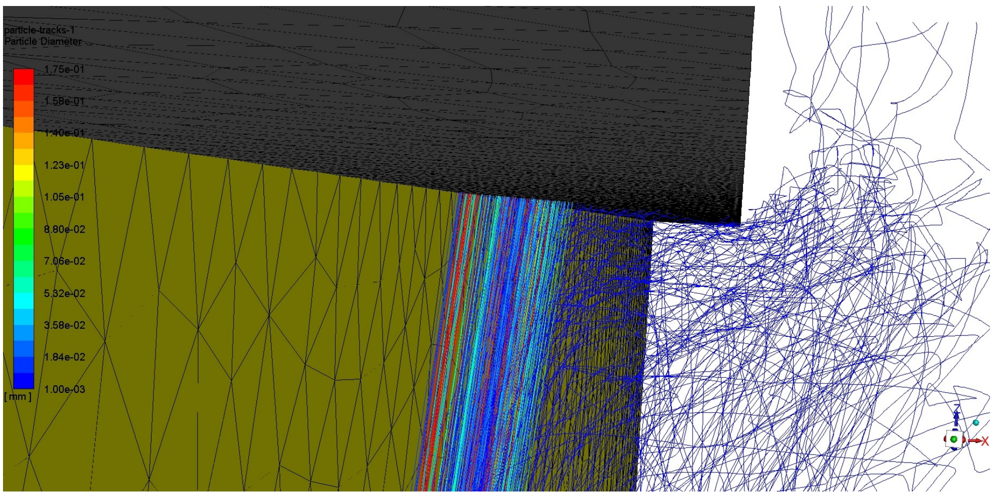

Figure 5.4: The particle trajectories that are captured on the substrate profile, the gray wall, with a particle release radius of 0.1 mm. The symmetry plane is shown in yellow. The contour of the particle trajectories describes the particle diameter and is between 0.001 mm and 0.175 mm going from blue to red

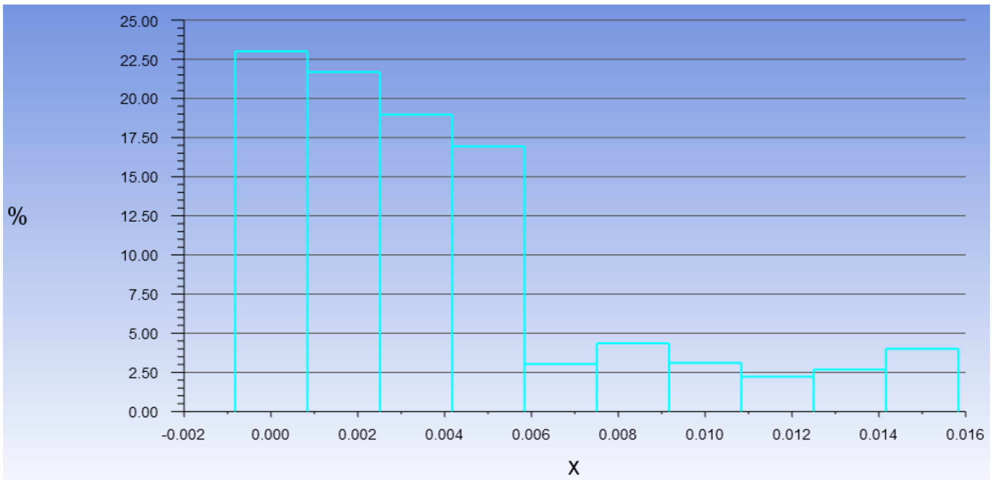

Figure 5.5: Histogram for a particle release radius of 0.1 mm, showing the percentage of particles being captured on the substrate profile with the x-axis being the width of the profile [m]

In figure 5.6 a release radius of 0.2 mm has been used and is visually showing wider spread. In the histogram in figure 5.7 it can be seen that a wider spread has been achieved though it does still not fully cover the profile.

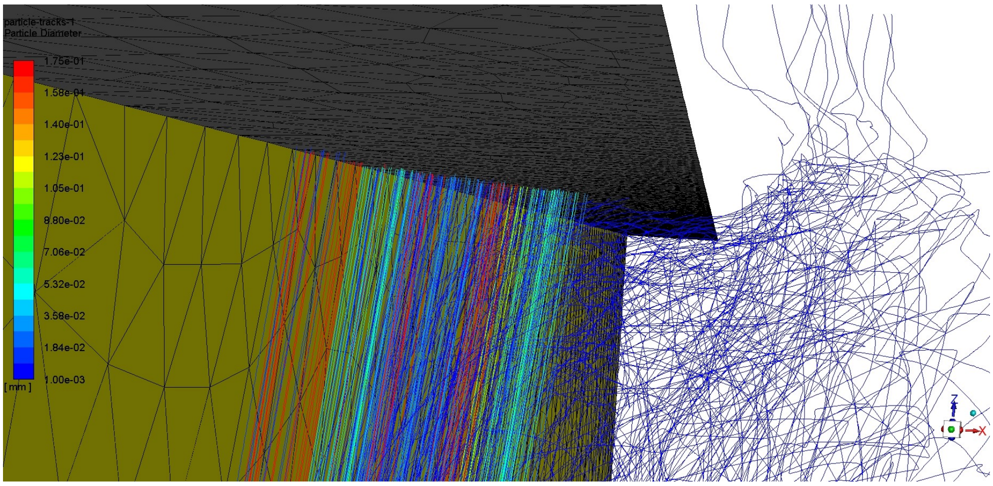

Figure 5.6: The particle trajectories that are captured on the substrate profile, the gray wall, with a particle release radius of 0.2 mm. The symmetry plane is shown in yellow. The contour of the particle trajectories describes the particle diameter and is between 0.001 mm and 0.175 mm going from blue to red

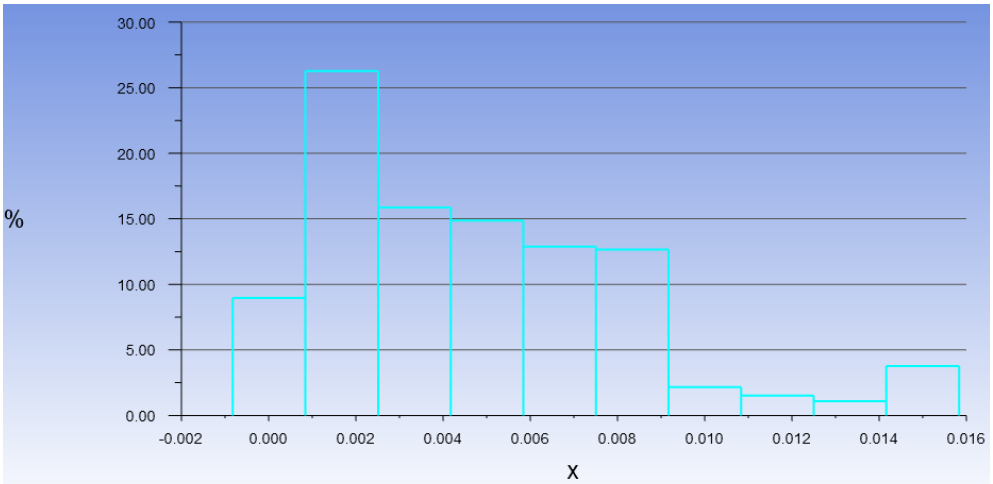

Figure 5.7: Histogram for a particle release radius of 0.2 mm, showing the percentage of particles being captured on the substrate profile with the x-axis being the width of the profile [m] and zero marking the center of the substrate profile

In figure 5.8 a release radius of 0.3 mm is used. A few of the larger particle diameters can be seen moving in a straight line past the profile. In figure 5.9 the histogram distribution that covers most of the profile although not the edge with a relatively even spread.

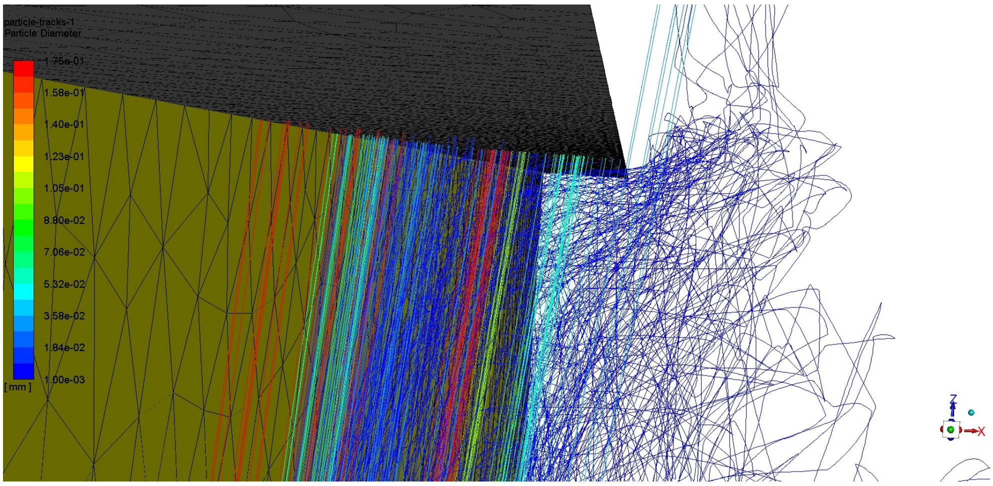

Figure 5.8: The particle trajectories that are captured on the substrate profile, the gray wall, with a particle release radius of 0.3 mm. The symmetry plane is shown in yellow. The contour of the particle trajectories describes the particle diameter and is between 0.001 mm and 0.175 mm going from blue to red

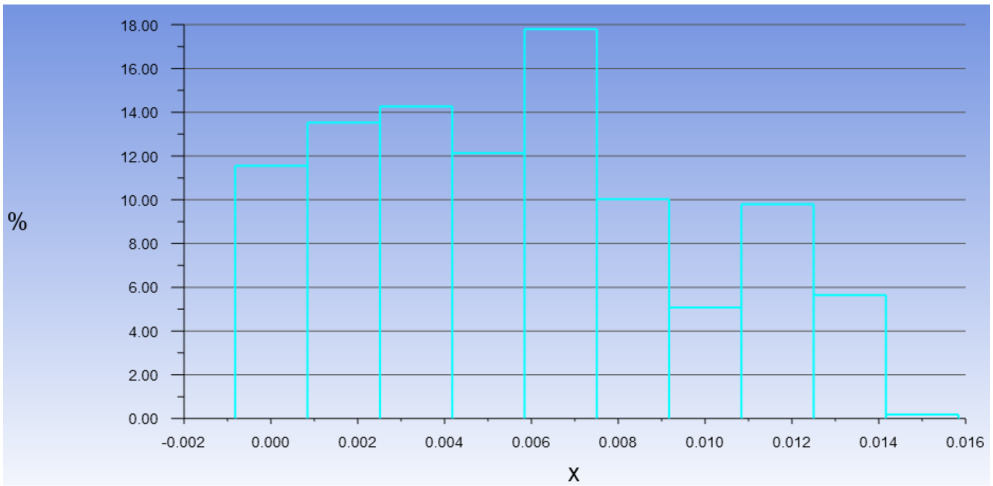

Figure 5.9: Histogram for a particle release radius of 0.3 mm, showing the percentage of particles being captured on the substrate profile with the x-axis being the width of the profile [m] and zero marking the center of the substrate profile

From figure 5.10 a spread of 0.4 mm has been used. Here it can be seen that a larger portion of the particles released misses the profile. This is unwanted as this will cause a loss in coating material. From figure 5.11 the histogram shows an uneven spread compared to the spread in 5.9.

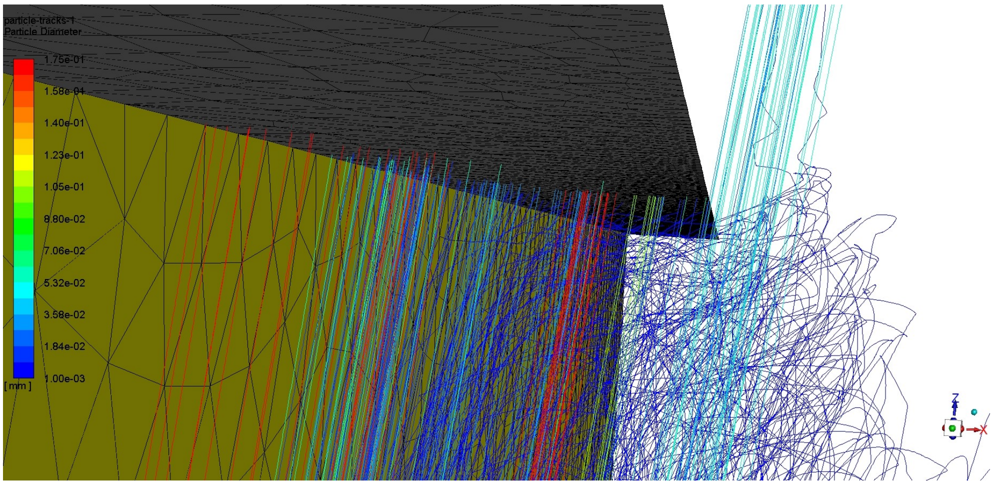

Figure 5.10: The particle trajectories that are captured on the substrate profile, the gray wall, with a particle release radius of 0.4 mm. The symmetry plane is shown in yellow. The contour of the particle trajectories describes the particle diameter and is between 0.001 mm and 0.175 mm going from blue to red

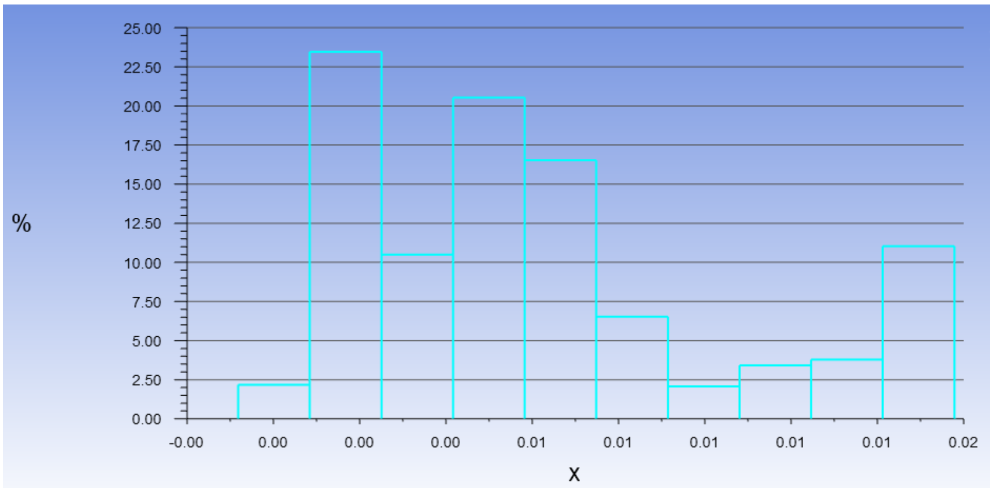

Figure 5.11: Histogram for a particle release radius of 0.4 mm, showing the percentage of particles being captured on the substrate profile with the x-axis being the width of the profile [m] and zero marking the center of the substrate profile

In figure 5.12 an even larger material loss can be observed when using a spread of 0.5 mm. In figure 5.13 the histogram shows that spread is uneven with a focus close to the middle of the profile.

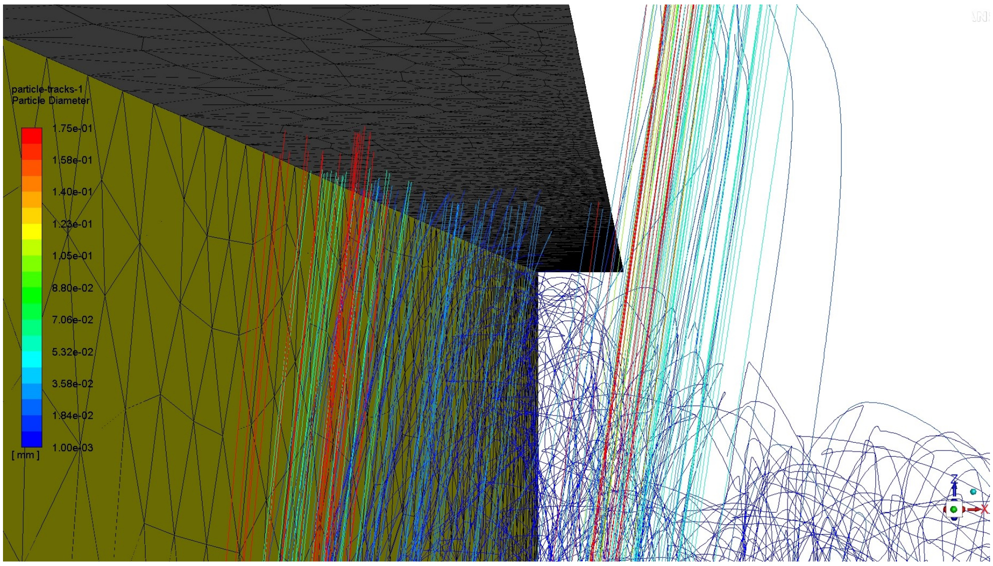

Figure 5.12: The particle trajectories that are captured on the substrate profile, the gray wall, with a particle release radius of 0.5 mm. The symmetry plane is shown in yellow. The contour of the particle trajectories describes the particle diameter and is between 0.001 mm and 0.175 mm going from blue to red

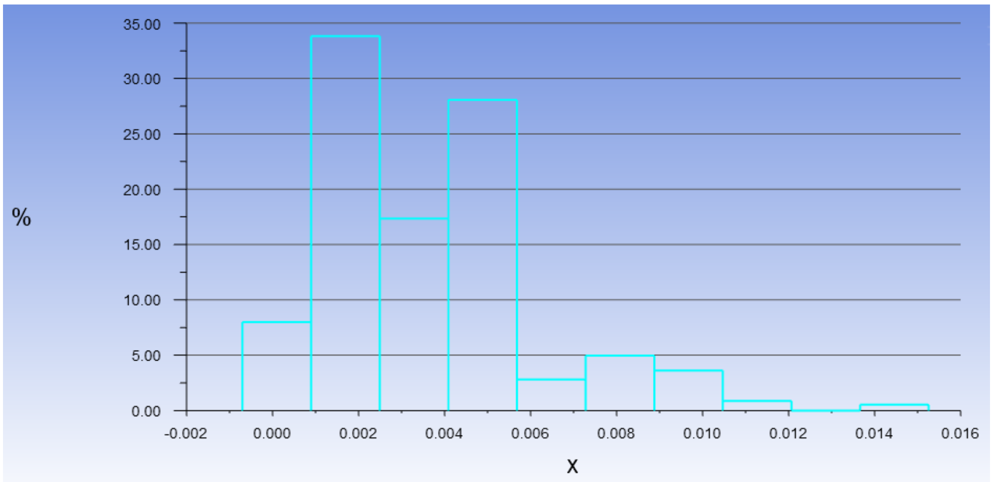

Figure 5.13: Histogram for a particle release radius of 0.5 mm, showing the percentage of particles being captured on the substrate profile with the x-axis being the width of the profile [m] and zero marking the center of the substrate profile

From comparing the results from the particle spread study with the experiment a particle release radius of 0.3 mm is chosen. This is done because a release radius of 0.3 mm is best able to emulate, what has been observed from the experiment.

5.3 Spray angle to the substrate profile

To investigate the effect of changing the spray angle the CAD model is changed in order to try and improve the coating quality. The angle that was used previously was at 60 degrees. The additional angles that will be investigated is 30, 45, and 75 degrees.

In figure 5.14 the particles being captured on the substrate profile can be seen with a spray angle of 30 degrees. In figure 5.15 the histogram shows that it has fewer particles covering the middle and edge of the profile, which is unfortunate as an even coverage is preferred.

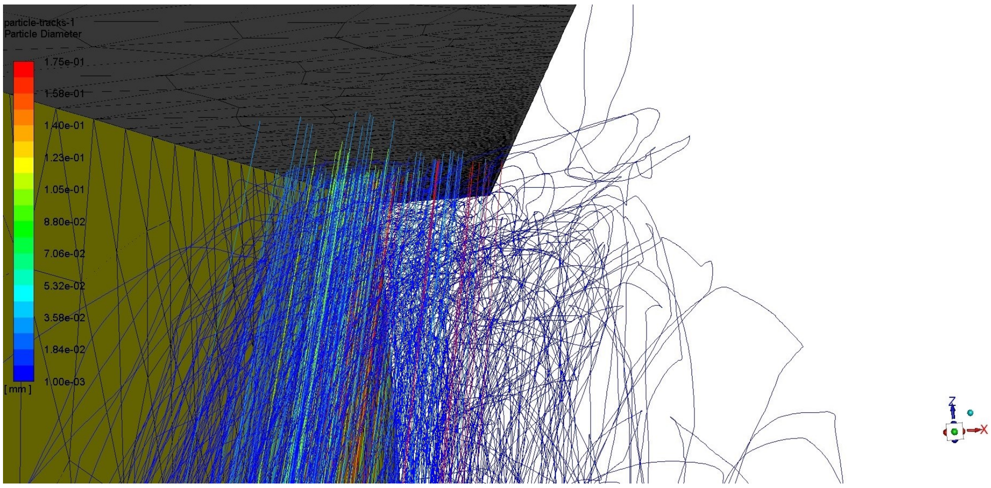

Figure 5.14: The particle trajectories that are captured on the substrate profile, the gray wall, with a spray angle of 30 degrees. The symmetry plane is shown in yellow. The contour of the particle trajectories describes the particle diameter and is between 0.001 mm and 0.175 mm going from blue to red

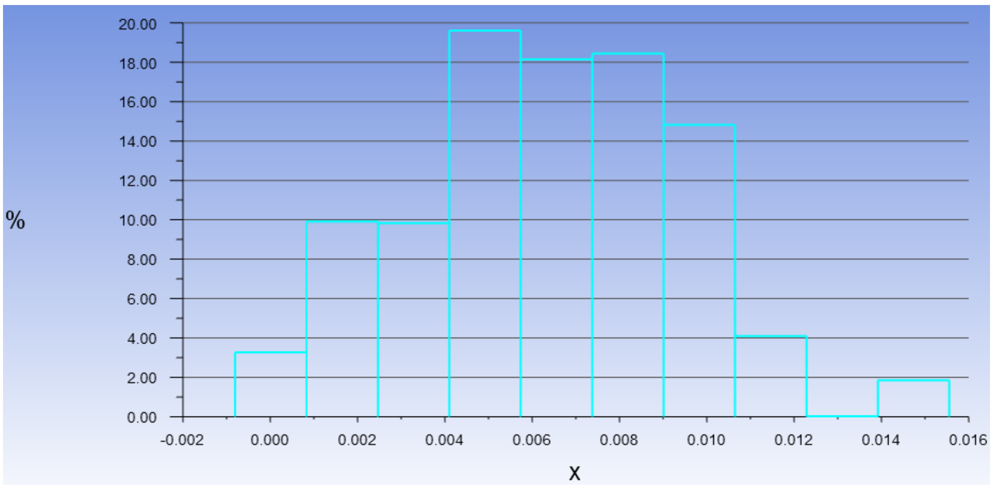

Figure 5.15: Histogram for a spray angle of 30 degrees, showing the percentage of particles being captured on the substrate profile with the x-axis being the width of the profile [m] and zero marking the center of the substrate profile

From figure 5.16 the particle path is seen going into the substrate profile with a spray angle of 45 degrees is used. From the histogram shown in figure 5.17 it can be seen it has a more even coverage than with a spray angle of 30 degrees. Though it is still not able to cover the edge.

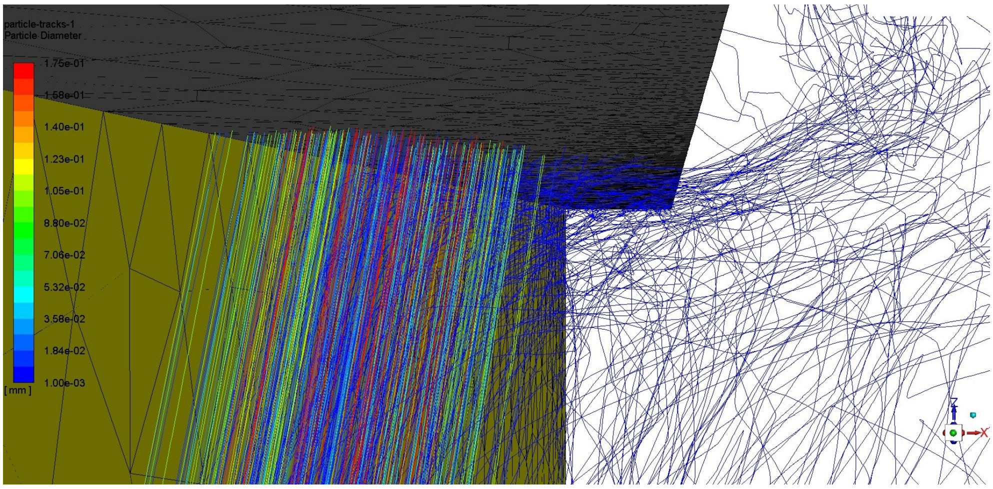

Figure 5.16: The particle trajectories that are captured on the substrate profile, the gray wall, with a spray angle of 45 degrees. The symmetry plane is shown in yellow. The contour of the particle trajectories describes the particle diameter and is between 0.001 mm and 0.175 mm going from blue to red

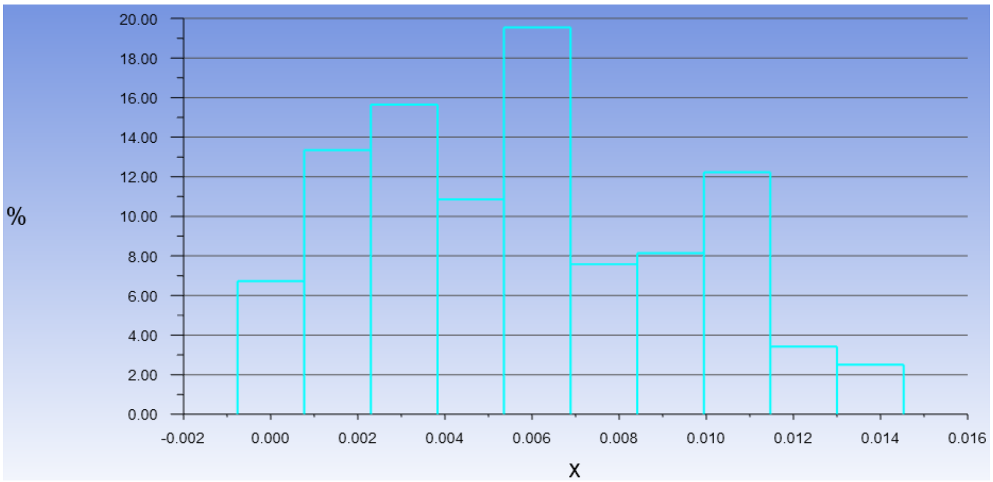

Figure 5.17: Histogram for a spray angle of 45 degrees, showing the percentage of particles being captured on the substrate profile with the x-axis being the width of the profile [m] and zero marking the center of the substrate profile

In figure 5.18 a spray angle of 75 degrees is used. The histogram in figure 5.19 show that it has an uneven particle spread, as it show peaks, which does not give an even coverage. To gain a better understand of any possible tendencies, it would be advantageous to simulate with a larger amount of particle trajectories.

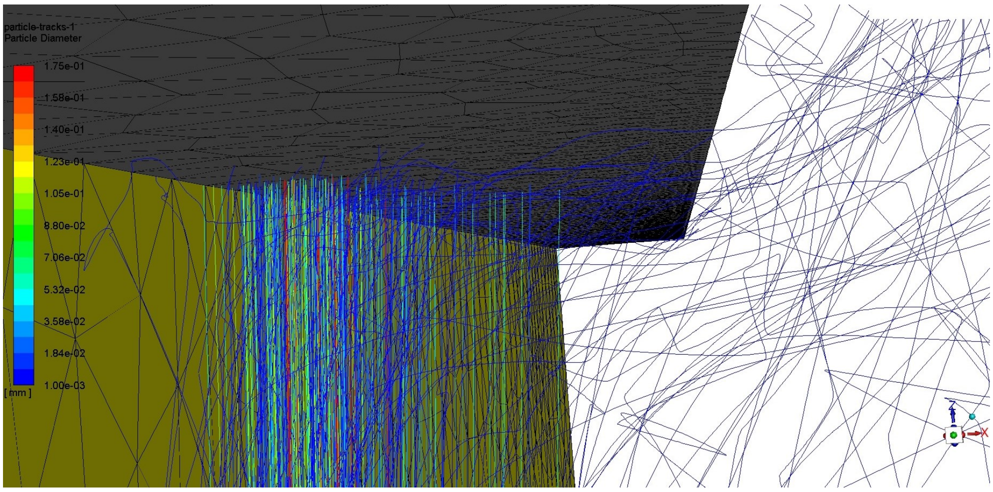

Figure 5.18: The particle trajectories that are captured on the substrate profile, the gray wall, with a spray angle of 70 degrees. The symmetry plane is shown in yellow. The contour of the particle trajectories describes the particle diameter and is between 0.001 mm and 0.175 mm going from blue to red

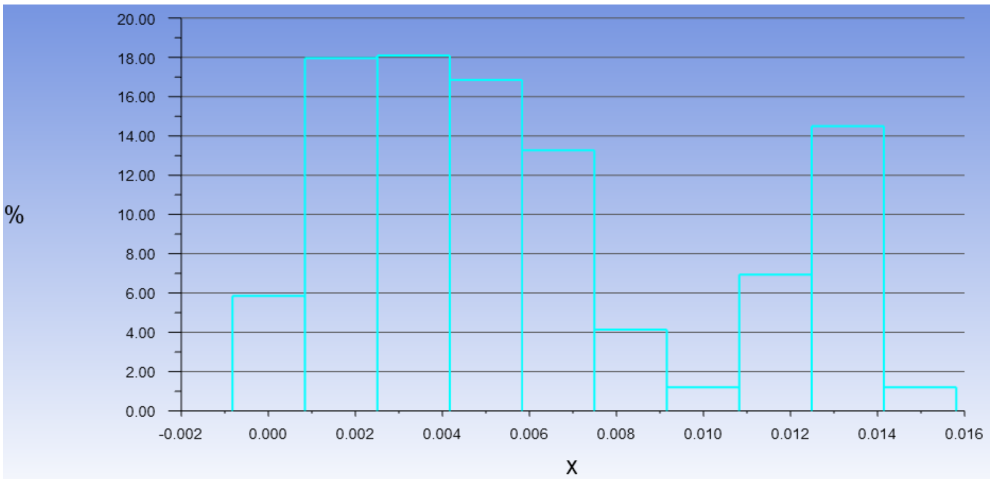

Figure 5.19: Histogram for a spray angle of 75 degrees, showing the percentage of particles being captured on the substrate profile with the x-axis being the width of the profile [m] and zero marking the center of the substrate profile

In figure 5.20 a spray angle of 60 degrees is used. This is the same angle used for the particle release radius study. From figure 5.21 the histogram show the most even coverage of the angles investigated.

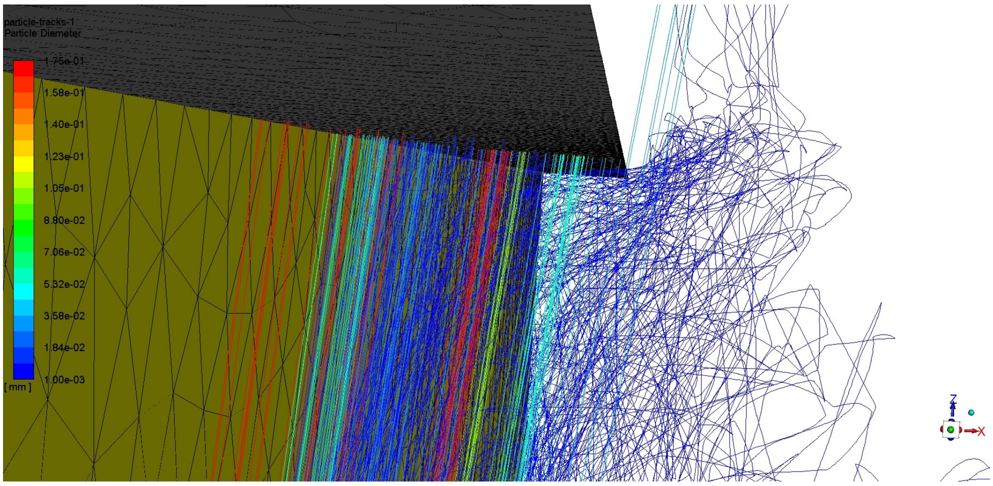

Figure 5.20: The particle trajectories that are captured on the substrate profile, the gray wall, with a spray angle of 60 degrees. The symmetry plane is shown in yellow. The contour of the particle trajectories describes the particle diameter and is between 0.001 mm and 0.175 mm going from blue to red

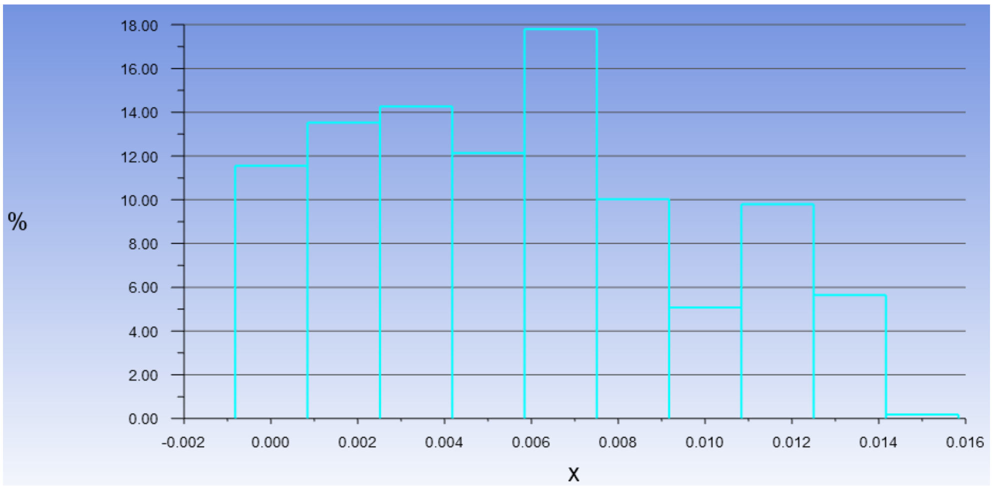

Figure 5.21: Histogram for a spray angle of 60 degrees, showing the percentage of particles being captured on the substrate profile with the x-axis being the width of the profile [m] and zero marking the center of the substrate profile

From these figures it can be deemed that a spray angle of 60 degrees gives the best coating quality of the angles that has been investigated.

5.4 Spray distance to the substrate profile

With the same goal of improving the coating quality, the effect of changing the spray distance is investigated. The different distances that are investigated are of 130 mm, 140 mm, and 150 mm, with 150 mm being the distance that has previously been used.

In figure 5.22 a spray distance of 130 mm has been used. From the histogram in figure 5.23 it can be seen that the majority of the particles are captured in the middle of the substrate profile.

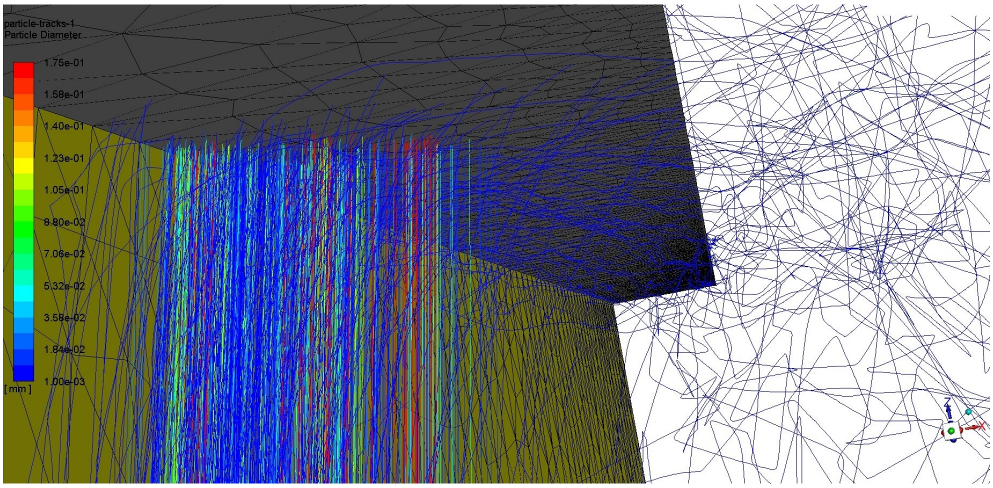

Figure 5.22: The particle trajectories that are captured on the substrate profile, the gray wall, with a spray distance of 130 degrees. The symmetry plane is shown in yellow. The contour of the particle trajectories describes the particle diameter and is between 0.001 mm and 0.175 mm going from blue to red

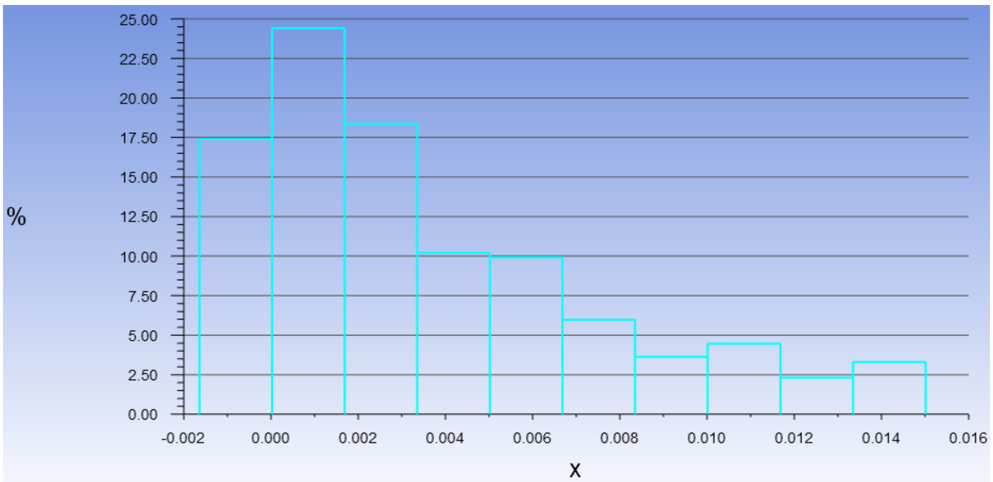

Figure 5.23: Histogram for a spray distance of 130 mm, showing the percentage of particles being captured on the substrate profile with the x-axis being the width of the profile [m] and zero marking the center of the substrate profile

With figure 5.24 a spray distance of 140 mm has been used. A small number of larger diameters can be seen moving past the profile. From figure 5.25 it can be seen that the particles are distributed relatively evenly.

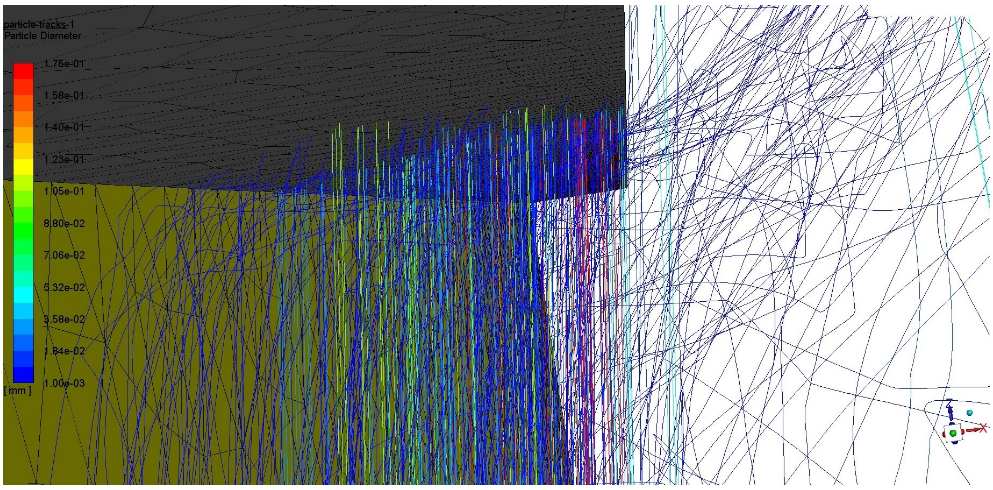

Figure 5.24: The particle trajectories that are captured on the substrate profile, the gray wall, with a spray distance of 140 degrees. The symmetry plane is shown in yellow. The contour of the particle trajectories describes the particle diameter and is between 0.001 mm and 0.175 mm going from blue to red

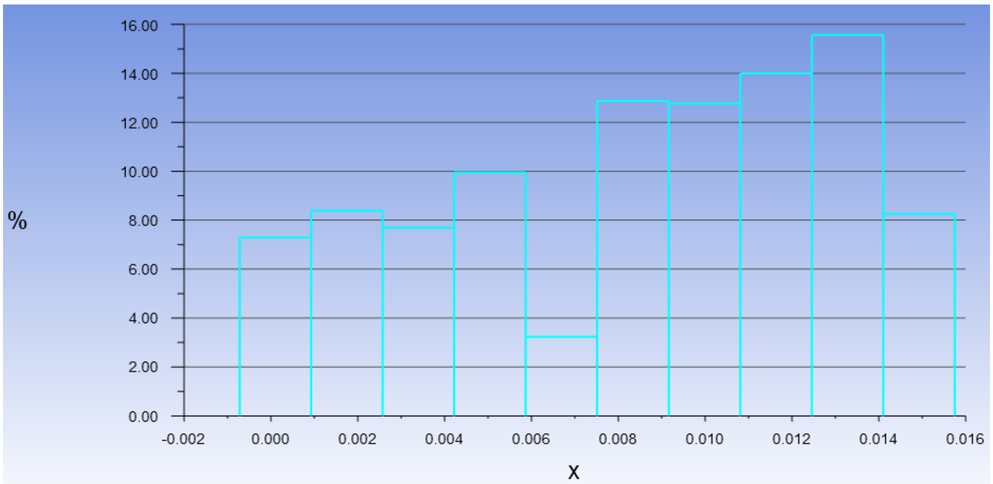

Figure 5.25: Histogram for a spray distance of 140 mm, showing the percentage of particles being captured on the substrate profile with the x-axis being the width of the profile [m] and zero marking the center of the substrate profile

In figure 5.26 a spray distance of 150 mm is used. This is the same distance as the one used for the particle release radius study.

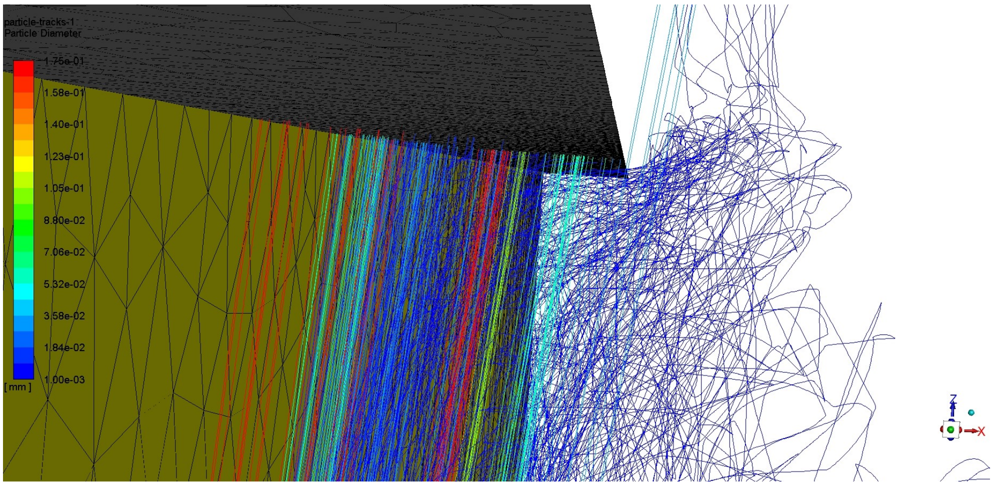

Figure 5.26: The particle trajectories that are captured on the substrate profile, the gray wall, with a spray distance of 150 degrees. The symmetry plane is shown in yellow. The contour of the particle trajectories describes the particle diameter and is between 0.001 mm and 0.175 mm going from blue to red

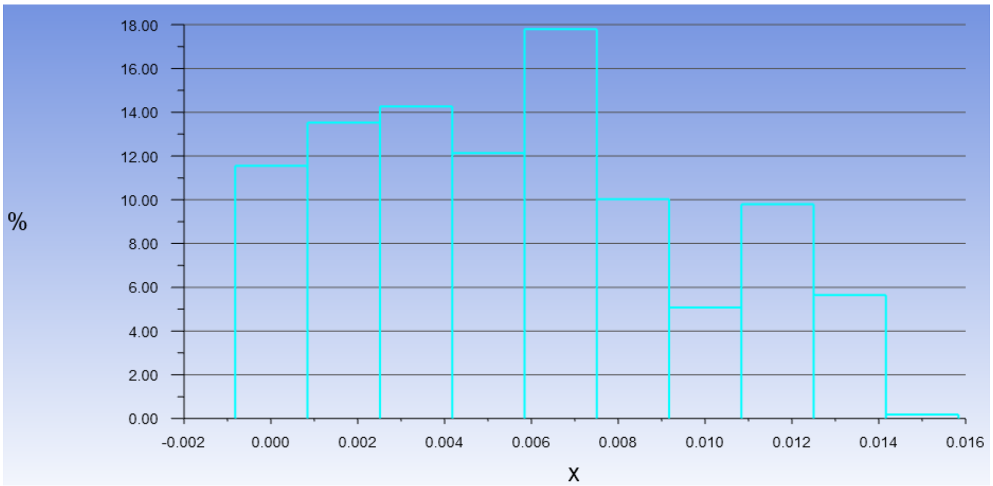

Figure 5.27: Histogram for a spray distance of 150 mm, showing the percentage of particles being captured on the substrate profile with the x-axis being the width of the profile [m] and zero marking the center of the substrate profile

From these different distances, a spray distance of either 140 mm or 150 mm shows the best coating coverage. The spray at 150 mm shows a possible difficulty of spraying the edge of the profile, whereas the spray at 140 mm is able to roughly cover the profile equally for its entire width.

6 Discussion

Through this study, a parametric study of a twin wire electric arc spraying process was conducted in respect to improving the coating quality. This was done through the use of a CAD model of the arc spray gun, and using ANSYS Fluent as the CFD modeling tool.

The CFD model was designed to emulate a possible production process, including a housing for the spraying process, the substrate that was sprayed upon, and a ventilation system which all was constructed as a CAD model. It was in the CAD model that any adjustment to the model was made.

The particle size distribution was constructed to emulate an existing study which constructed a Rosin-Rammler size distribution. Using this particle size distribution in Fluent a spray width wide enough to cover the profile was found to be achievable with a particle release radius of 0.3 mm.

With the use of this particle release radius the study investigated the effect of changing the spray angle. From this an angle of 30 degree was found to not be able to cover the middle and edge of the profile. An angle of 45 degree showed a better spread although some unevenness still appear, and still not being able to fully cover the edge of the profile. A spray angle of 60 degree showed a more evenly coating spread, though still not reaching the edge. The last angle of 75 degree also showed an uneven spread with areas with less coverage. From these angles a spray angle of 60 degree was deemed the option that was best at covering the substrate profile.

Using this spray angle the study investigated the effect of changing the spray distance. Using a spray distance of 130 mm the coating coverage seems to be focused near the middle of the profile, which is undesirable as an even coverage is desired. With a spray distance of 140 mm an relatively even coverage can be achieved with just a single area being significantly lower than the other areas. From a distance of 150 the coverage also seem even, though not being able to fully cover the edge. From these distances it can be deemed that a spray distance of 140 mm gives the coating with the most evenly distributed coating material.

Using this study it has been deemed that a spray angle of 60 degree and a spraying distance of 140 mm gives the best coating coverage, which should give the most optimal coating quality.

6.1 Further study

To improve upon this study a more detailed investigation can be made through having smaller changes in angle and distance. At the same time changing both the angle and distance can give insight into another setup that possibly would be able to achieve an even smoother coating. Another area that would be relevant to investigate would be finding the amount of particles not being trapped in the substrate profile, as this would give an insight into the possible material waste.

To further optimize upon the spray gun construction an investigation into specific areas could be made. Seeing if changing nozzle's angle and distance to the particle release has an effect on the particle spread. Investigating if an added shaping of the air cap can shape the air flow to improve the particle spread for certain parameters.

6.2 Conclusion

From this study it has been possible to determine the optimal spraying distance and spraying angle, when spraying onto a specific substrate profile with conditions emulating a possible production process. Through the use of ANSYS Fluent a CFD model was used to produce data able to illuminate which changes show an improvement when focusing on the simulations ability to coat the substrate profile and thereby optimize this specific construction.

Bibliography

[1] Stefan Lucian Toma et al. „The effect of frontal nozzle geometry and gas pressure on the steel coating properties obtained by wire arc spraying“. In: *Surface & Coatings Technology* 220 (2013), pp. 266–270.

[2] I. Gedzevicius and A. V. Valiulis. „Analysis of wire arc spraying process variables on coatings properties“. In: *Journal of Materials Processing Technology* 175 (2006), pp. 206–221.

[3] Yongxiong Chen et al. „Numerical analysis of the effect of arc spray gun configuration parameters on the external gas flow“. In: *Journal of Materials Processing Technology* 209 (2009), pp. 5924–5931.

[4] Joël Fournier, Danielle Miousse, and Jean-Gabriel Legoux. „Wire-arc sprayed nickel based coating for hydrogen evolution reaction in alkaline solutions“. In: *International Journal of Hydrogen Energy* 24 (1999), pp. 519–528.

[5] Rongguo Wang et al. „Effect of arc spraying power on the microstructure and mechanical properties of Zn-Al coating deposited onto carbon fiber reinforced epoxy composites“. In: *Applied Surface Science* 257 (2010), pp. 203–209.

[6] A. P. Newbery, T. Rayment, and P. S. Grant. „A particle image velocimetry investigation of in-flight and deposition behaviour of steel droplets during electric arc sprayforming“. In: *Materials Science and Engineering A* 383 (2004), pp. 137–145.

[7] Hongying Li, Junying Duan, and Xiaobing Min. „Comparative studies on the initial stage of arc-sprayed and zinc-rich powder coatings in sulfur-rich environment“. In: *Alloys and Compounds* 616 (2014), pp. 14–25.

[8] Krishnarao Venugopal and Manish Agrawal. „Evaluation of arc sprayed coatings for erosion protection of tubes in atmospheric fluidised bed combustion (AFBC) boilers“. In: *Wear* 264 (2008), pp. 139–145.

[9] T. van Hooff, B. Blocken, and Y. Tominaga. „On the accuracy of CFD simulations of cross-ventilation flows for a generic isolated building: Comparison of RANS, LES and experiments“. In: *Building and Environment* 114 (2017), pp. 148–165.

[10] Clayton T. Crowe et al. *Multiphase Flows with Droplets and Particles*. Ed. by NA. 2nd. CRC Press, 2012.

[11] Rodolphe Bolot et al. „A three-dimensional model of the wire-arc spray process and its experimental validation“. In: *Journal of Materials Processing Technology* 200 (2008), pp. 94–105.

[12] Clayton Crowe, Martin Sommerfeld, and Yutaka Tsuji. *Multiphase Flows with Droplets and Particles*. 1st ed. CRC Press, 1997.